Journal of Digital Imaging

Development and Validation of Automated 2D–3D Bronchial Airway Matching to Track Changes in Regional Bronchial Morphology Using Serial Low-Dose Chest CT Scans in Children with Chronic Lung Disease

Pavithra Raman,[1] Raghav Raman,[2] Beverley Newman,[2] Raman Venkatraman,[1] Bhargav Raman,[2] and Terry E. Robinson[1]

To address potential concern for cumulative radiation exposure with serial spiral chest computed tomography (CT) scans in children with chronic lung disease, we developed an approach to match bronchial airways on low-dose spiral and low-dose high-resolution CT (HRCT) chest images to allow serial comparisons. An automated algorithm matches the position and orientation of bronchial airways obtained from HRCT slices with those in the spiral CT scan. To validate this algorithm, we compared manual matching vs automatic matching of bronchial airways in three pediatric patients. The mean absolute percentage difference between the manually matched spiral CT airway and the index HRCT airways were 9.4±8.5% for the internal diameter measurements, 6.0±4.1% for the outer diameter measurements, and 10.1±9.3% for the wall thickness measurements. The mean absolute percentage difference between the automatically matched spiral CT airway measurements and index HRCT airway measurements were 9.2±8.6% for the inner diameter, 5.8±4.5% for the outer diameter, and 9.9±9.5% for the wall thickness. The overall difference between manual and automated methods was 2.1±1.2%, which was significantly less than the interuser variability of 5.1±4.6% ($p<0.05$). Tests of equivalence had $p<0.05$, demonstrating no significant difference between the two methods. The time required for matching was significantly reduced in the automated method ($p<0.01$) and was as accurate as manual matching, allowing efficient comparison of airways obtained on low-dose spiral CT imaging with low-dose HRCT scans.

KEY WORDS: 3D imaging (imaging, three-dimensional), algorithms, chest CT, computer analysis, image analysis, image processing, image registration, imaging, three-dimensional, lung diseases, lung, radiation dose, reproducibility of results

BACKGROUND

To assess progression of chronic lung diseases such as cystic fibrosis (CF), several authors have utilized serial chest high-resolution computed tomography (HRCT) or spiral CT scans to evaluate changes with interventions or to follow up the natural progression of CF lung disease.[1–19] In the last 10 years, multidetector CT scanners have become available for most hospitals, providing spiral chest CT scans of the entire lungs in less than 10 s in children while still providing the capability of doing HRCT imaging. These scanners allow adjustment of CT dose parameters to limit radiation exposure. For example, the calculated effective dose utilizing the ImPACT CT dosimetry tool[20] and pediatric dosimetry formula provided by Huda and Ogden[21] in a 10-year-old boy for combined low-dose inspiratory and expir-

[1]*From the Department of Pediatrics, Stanford University School of Medicine, Stanford, CA 94305-5105, USA.*

[2]*From the Department of Radiology, Stanford University School of Medicine, Stanford, CA 94305-5105, USA.*

Electronic supplementary material *The online version of this article (doi:10.1007/s10278-009-9199-3) contains supplementary material, which is available to authorized users.*

Correspondence to: Terry E. Robinson, Department of Pediatrics, Stanford University School of Medicine, Stanford, CA 94305-5105, USA; tel: +1-650-4987603; fax: +1-650-4986345; e-mail: ter@stanford.edu

Online publication 15 September 2009

doi: 10.1007/s10278-009-9199-3

atory spiral CT imaging is 1.6–2.2 mSv (peak X-ray tube voltage, 100 kVp; tube current second, 40 mAs; collimation, 0.6 mm; pitch, of 1.4 to 1.0; Z-length, 28 cm inspiratory and 25 cm expiratory). This represents an approximate 75% reduction in the calculated effective dose for this low-dose spiral CT protocol compared to previously utilized standard inspiratory and expiratory spiral CT imaging (6.2–8.8 mSv for 120 kVp peak X-ray tube voltage, 100 mAs tube current second, 0.6 mm collimation, 1.4–1.0 pitch, and 28 cm and 25 cm Z-length for inspiratory and expiratory spiral scans).[20,21] Decreases in the effective dose for HRCT imaging can also be obtained by using low-dose HRCT protocols compared to standard HRCT protocols. In a 10-year-old boy using a low-dose inspiratory/expiratory HRCT protocol (100 kVp peak X-ray tube voltage, 40 mAs tube current second, 0.6 mm collimation, 2×1.0 mm every 10 mm from apex to base of lung), the calculated effective dose is 0.27 mSv. This also represents a 75% reduction in radiation exposure using this low-dose protocol compared to the standard HRCT protocol (1.10 mSv for 120 kVp peak X-ray tube voltage, 100 mAs tube current second, 0.6 mm collimation, 2×1.0 mm every 10 mm from apex to base of lung).[20,21]

Despite these advances in scanner technology, which reduces scanning time and potential radiation dose, there is potential concern for cumulative radiation exposure if multiple low-dose spiral CT (LDSCT) scans are used to follow up children with chronic lung disease over time in the clinical setting. To address this important issue in clinical chest imaging, we propose an approach of utilizing alternating LDSCT scans with 1- or 2-year follow-up low-dose HRCT (LDHRCT) scans for serial evaluations of children with progressive chronic lung disease. While two serial LDSCT scans would result in a total dose of 3.2–4.4 mSv, a LDSCT scan and a LDHRCT scan results in a total dose of 1.8–2.5 mSv. This approach would therefore further reduce radiation dose by approximately 44%.

Multidetector CT has become a powerful tool for evaluating disease progression or effects of therapeutic interventions in chronic diseases such as CF. Multidetector CT has been used in 3D evaluation of structural changes in the tracheobronchial airways as a result of chronic pulmonary diseases.[17,22–24] In CF, these changes have been evaluated by chest CT scoring systems[6,7,12–14,17–19,25–32] and more recently by quantitative measurements of airways[11,33,34] and air trapping[35–37] obtained from either chest HRCT imaging or spiral chest CT techniques. In addition, quantitative airway measurements have also been determined in other chronic lung diseases using similar techniques.[38–44] Quantitative indices of bronchial airway morphology, including airway diameters, wall thicknesses, wall area, airway segment lengths, airway taper indices, and airway branching patterns can be calculated.[38–49] We have previously developed an integrated software package that enables the user to perform automated segmentation, measurement, and database archiving of bronchial morphology using spiral CT scans, reducing the processing time per scan.[45] We aimed to extend the application of this software to match and measure bronchial airways taken from LDHRCT scans with those from LDSCT scans.

In a LDHRCT scan, fewer optimally circular bronchi can be measured from each slice of the HRCT scan. This may yield 20–30 or more bronchial airway measurements for the whole lung. To compare this small set of bronchial measurements, a high degree of accuracy has to be achieved in matching the airways seen in the LDHRCT images to the same airways identified on a LDSCT. This is crucial in ensuring that small changes in airway morphology are evident and in avoiding errors due to approximate matching. Other registration algorithms for the structures within the lung are not specifically designed to match airway cross-sections between scans, do not take into account the inherent problem of matching the position and orientation of a specific airway cross-section in serial scans, and do not take advantage of the anatomy of the bronchial tree and surrounding structures to achieve better registration.[50–56] We therefore aimed to produce an algorithm that allows specific bronchi in LDHRCT scans to be matched to the same bronchi seen in a prior or follow-up LDSCT scan with accuracy that is comparable to manual matching.

METHODS

Automated Algorithms

The full automation of 3D bronchial tree analysis was achieved through the development

of several interlinked algorithms that are described in a previous paper.[45] These algorithms, when applied to an initial volumetric scan, yielded a tracheobronchial segmentation. This segmentation was used to generate a tree structure that consisted of branching paths through the segmented airways. Each bronchial segment was then extracted, and a semi-automated method was used to apply anatomic labels to the segments. In any part of the bronchial tree, this system allowed the inner and outer diameter of the bronchus to be determined and wall thickness and other morphological measures to be calculated.

Automated Matching of Bronchi

The matching algorithm (Fig. 1) allows users to select the center of a bronchial airway cross-section in the LDHRCT scan (the target bronchus). Our previously described bronchial airway algorithm[45] is first used to calculate the inner and outer perimeters of the target bronchus. Then, a field of view for matching is selected, which is defined as four times the diameter of the target bronchus at the measurement position and orientation (rounded to the nearest 5 mm). Within this field of view, the center point of the target bronchus is then determined. Three hundred and sixty radial spokes are then generated from the center of the target bronchus. The radial spokes traverse the outer perimeter of the target bronchus and continue to be propagated until air intensity voxels are encountered. The "visible surround perimeter" of the target bronchus is defined as the contour traced by the tips of the radial spokes after they have completed their propagation. The voxels contained within the visible surround perimeter and external to the outer perimeter of the bronchus is termed the "visible surround" of the bronchus. All other soft tissue intensity voxels within the field of view are defined as the "non-visible surround" (Fig. 2). Using connected component analysis, the perimeter of the non-visible surround voxels is extracted. Small connected components are excluded from the analysis. Following this, the visible surround perimeter and non-visible surround perimeter are saved to a data file. To match the position of the target bronchus to the LDSCT scan, the LDSCT scan is opened in a separate instance of our software. The segmentation and airway tree specific to this scan is then loaded. When the matching algorithm is run, the data file that contains the visible surround perimeter and non-visible surround perimeter for the target bronchus is loaded. The visible surround perimeter and non-visible surround perimeter for the bronchial cross-sections in the LDSCT scan are then determined every 1 mm along the middle 80% of the length of all airway segments (candidate bronchi). The data thus obtained are then used to find the candidate bronchus that best matches the target bronchus, as described below. First, for each candidate bronchus, rotational and translational registration offsets are calculated, and finally, the resulting data are then used to calculate a match score for each candidate bronchus. The candidate bronchus with the lowest match score is selected as the best match bronchus. A more detailed description of these steps is provided below.

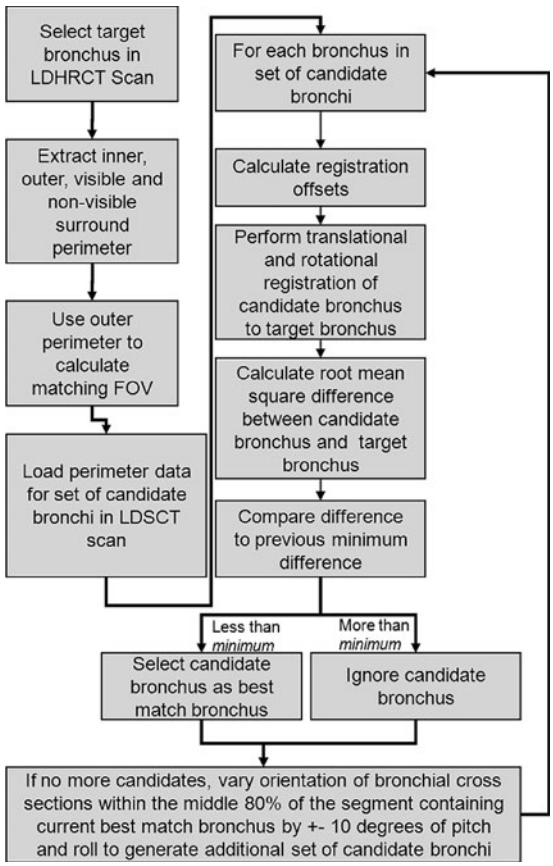

Fig 1. Algorithm flowchart. The algorithm is initiated by the user selecting a target bronchus in the LDHRCT scan. The algorithm then iterates through the set of candidate bronchi in the LDSCT to find the bronchus with the lowest match score, which is then selected as the best automatic match bronchus.

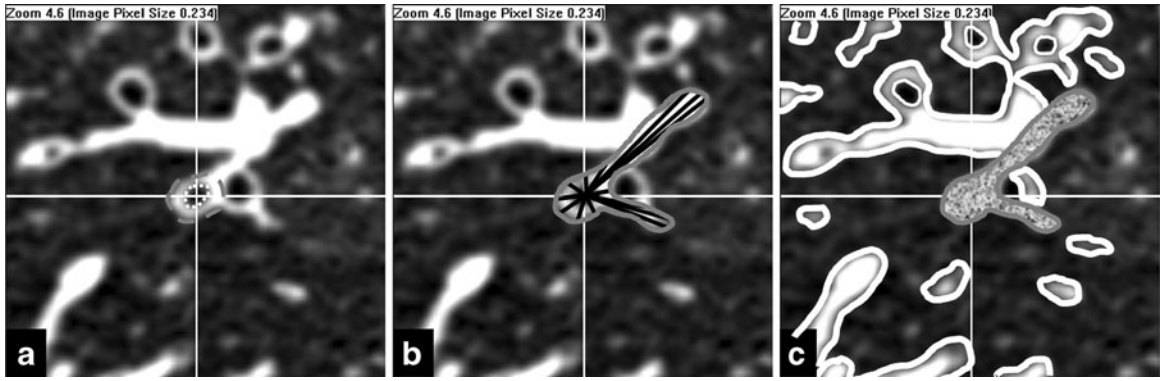

Fig 2. Extraction of perimeters. a The candidate bronchus is selected and the center of the bronchus is found. The inner (*dotted white*) and outer (*dashed gray*) perimeters are delineated. b The visible surround perimeter is then defined as the contour traced by the tips of the radial spokes (*black*) after they have completed their propagation. A total of 360 radial spokes are generated but only a few are shown. c After the visible surround perimeter has been defined (*solid gray*) using connected component analysis, the non-visible surround perimeter (*solid white*) is then calculated. Small connected components are excluded from the analysis.

Calculation of Registration Offsets

To determine the translational offsets, the aggregate center of mass point of the inner and outer perimeters of the candidate bronchus is calculated. The aggregate center of mass of the inner and outer perimeters of the candidate bronchus is translated to the center of mass calculated from the target bronchus. Following this, a line is drawn from the aggregate center of mass of the inner and outer perimeter to the center of mass of the visible surround perimeter for both the candidate bronchus and the target bronchus. The angle between the lines drawn for the candidate bronchus and the target bronchus is defined as the rotational correction factor. The data for the candidate bronchus are then rotated by this angle to register the data to that of the target bronchus (Fig. 3).

Scoring

Each candidate bronchus is evaluated for its similarity to the target bronchus after translational and rotational registration is performed. A root mean square difference in millimeter is calculated between the visible surround perimeters of the target bronchus and that of the candidate bronchus. Then, a root mean square difference in millimeter is calculated between the outlines of the non-visible surround perimeters of the target bronchus and that of the candidate bronchus. For the calculation of the overall match value, a weighting factor of 2 is given to the root mean square difference between the visible surround perimeters and 1 to the root mean square difference between the non-visible surround perimeter. The visible surround perimeter is the most irregular and most characteristic of the bronchus. It includes the wall of the bronchus and the nearby lymph nodes and blood vessels that are close enough to appear to be attached to the wall. In addition, soft tissue and the visible parts of the bronchi that are adjacent to the bronchus to be matched are also included in calculating this visible surround perimeter. Hence, this feature is given the higher weighting factor. The non-visible surround perimeter then represents the soft tissue components that are within the small field of view (4 times the diameter of the bronchus) selected around the bronchus. These elements, being farther away from the bronchus, are important in matching the orientation and position. This is because with small changes in orientation and position, these elements being farther away from the walls of the bronchus will be affected more than the elements close to the bronchus. However, this feature is also variable and is more dependent on scan protocol. Hence, this feature was given the lower weighting factor.

Search

Data related to candidate bronchi, such as the visible surround perimeter and the non-visible surround, are calculated once per candidate bronchus, and the data are cached so that subsequent searches do not have to recalculate this data. All candidate bronchial cross-sections along the cen-

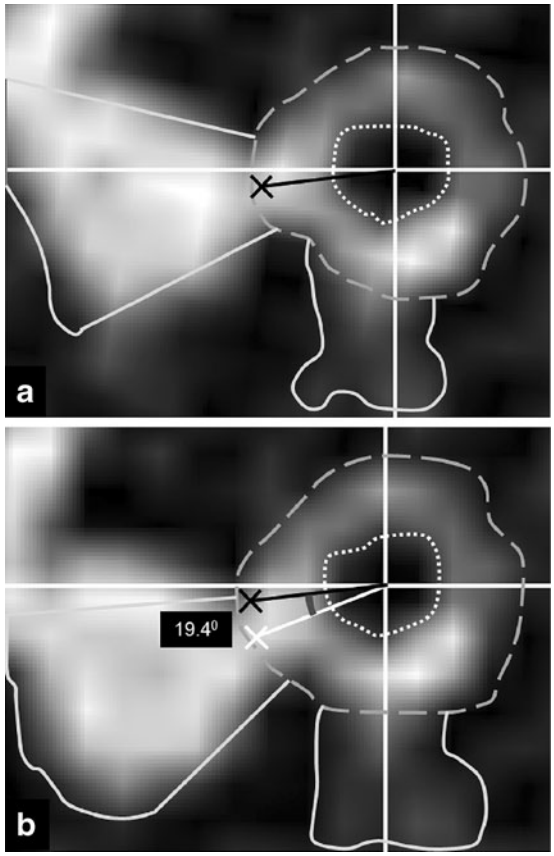

Fig 3. Calculation of registration offsets. Images showing the inner (*dotted*), outer (*dashed*), and visible surround (*solid*) perimeters of the target bronchus (a) and candidate bronchus (b). The aggregate center of mass of the inner and outer perimeters are marked by the *white crosshairs* in a and b. The data for the candidate point are first translated by an amount equal to the offset between the aggregate centers of mass of the inner and outer perimeters. The aggregate center of mass of the visible surround perimeter is marked as a *black cross* for the target bronchus and a *white cross* for the candidate bronchus. In a, a *black line* is drawn from the aggregate center of mass of the inner and outer perimeter to the center of mass of the visible surround perimeter. In b, a *white line* is drawn from the aggregate center of mass of the inner and outer perimeter to the center of mass of the visible surround perimeter. The *black line* from a is projected onto b. The angle between these lines is calculated as the rotational correction factor, in this case 19.40. The data for the candidate point are then rotated by this angle to register the data to that of the target point before a match score is calculated.

terline of the middle 80% of all bronchial segments are compared with an orientation that is close to the axial orientation, and a match score for each is obtained using the above algorithm. The candidate bronchus with the lowest match score is then selected as the point with the most likelihood of being within the same segment as the target bronchus. Following this, the bronchi within the segment are searched as follows. All bronchi within the segment are chosen, and the orientation of the cross-section obtained is varied by ±10° in the pitch and roll directions with step size of 1°. The candidate bronchial cross-section with the position and orientation within the middle 80% of the segment that yields the smallest match value is then selected. This approach would match bronchi even in the context of patient growth. Patient growth mainly results in increase in the size of the structures being matched, but the general shape of the structures being matched will remain similar. Small changes in the shape result in large mismatches between the candidate and target bronchus, but small changes in size result in a mismatch that is only proportional to the change in size. Since this change in size is expected to be more or less similar throughout the lung, the amount of mismatch due to a change in size will also be similar for all candidate bronchi. Therefore, the algorithm would still be very biased toward selecting the best match with respect to shape.

Validation

To validate this algorithm, we selected three pediatric patients with CF (ages 6, 7, 15 years on initial CT scans) who had a LDSCT scan and also a LDHRCT scan at different dates available on our Picture Archiving and Communications System obtained under a protocol approved by our institutional review board. Comparisons were made on LDHRCT and LDSCT scans. All LDSCT scans were performed with low-dose protocols at 100 kVp and 80 mA (40 mAs) with 0.6-mm slice thickness and 50% overlap and a pitch of 1.0. LDHRCT scans were performed at 100 kVp and 60–80 mA (30–40 mAs) with 2×1 mm slice thickness and 10 mm spacing between HRCT slice sets. The first and second patients' LDHRCT and LDSCT scans were spirometer-gated, while the third patient's LDSCT scan was spirometer-gated, but the follow-up LDHRCT scan was obtained by volitional breath hold maneuver after practicing breathing technique to assure full inflation. The first patient's LDHRCT scan was completed in August 2006 at 91% of the patient's supine slow vital capacity (SVC). The LDSCT scan was done in December 2007 at 85% of the patient's SVC. The second patient's LDHRCT scan was done in May 2006 at 95% of the SVC, and the LDSCT scan

was done in August 2007 at 100% of the SVC. The third patient had a LDSCT scan that was spirometer-gated in August 2007 at 95% of the patient's SVC, while the follow-up LDHRCT scan in December 2007 was obtained at a practiced full inflation.

Comparison Between Manual Matching and Automatic Matching

To validate our automated matching technique, we compared manual matching by two radiologists (pediatric thoracic radiologist with over 15 years experience in thoracic imaging and a trained radiology resident with over 5 years experience in thoracic imaging) and one trained CT research technician with automatic matching using our algorithm. A computer with a Core2Duo (Intel, Santa Clara, CA, USA) 1.86 GHz processor and 4 GB of RAM was used to run the automated algorithm. The three raters were asked to select bronchi seen in cross-section on the LDHRCT scans. All bronchi from apical to base HRCT slices that had a maximum diameter to minimum diameter ratio of 1–1.2 were accepted for measurement, which would correspond to bronchi that were nearly perpendicular to the axial scan plane. This therefore limited the number of bronchial airways that could be evaluated. The bronchi that were selected were distributed throughout the lung parenchyma. The raters selected every acceptable visible bronchus within each LDHRCT slice (termed the index bronchus) and measured the bronchial luminal diameter and wall thickness using our previous described methodology.[42] Subsequently, the rater attempted to manually locate the exact same position and orientation of the bronchus in the LDSCT scan to obtain the best match with the index bronchus (henceforth referred to as the manual match bronchus). The time for manual matching of airways was also recorded. Subsequently one rater, blinded to previous airway matches, activated the automated matching algorithm, which then gave as output the measurement with the lowest match score (henceforth referred to as the automatic match bronchus). The time required to run the automated algorithm was also recorded.

Statistical Analysis

Between rater reliability for the three raters for manual matching of the index airways on LDHRCT scans with those noted on the LDSCT scan was obtained using the Shrout–Fleiss intraclass correlation for three raters.[57] The percentage difference between index LDHRCT and manual match LDSCT scan measurements for inner diameter, outer diameter, and wall thickness were calculated between the manual match measurement and the index (LDHRCT) measurement, and results for all three raters were then averaged. The percentage difference between the index LDHRCT measurement and automatically matched LDSCT measurements were also determined for inner diameter, outer diameter, and wall thickness. The variability between automated and manual methods was compared to the interuser variability for the manual method for the three raters using a paired t test. Schuirmann's two one-sided equivalence test with a paired design[58] was used to test the null hypothesis that there is a difference between the measurements for manual and automatic methods. The maximum acceptable difference in the calculated percentage difference between LDSCT and LDHRCT scans that was considered clinically unimportant was set to <5%, which is comparable to the mean interuser variability between manual raters. For each of the individual statistical tests comprising the Schuirmann's test, a p value of <0.025 was considered to be significant. Finally, the time required for automated and manual matching was compared using a paired t test to test the null hypothesis that there was no significant difference between the time taken to perform the automated and manual matching methods. A p value of <0.05 was considered significant for the statistical analyses described above.

Results

Seventy-five index bronchi were selected for analysis in the three patients with CF, representing a mean of 25 index bronchi per patient. The selected index bronchi had a mean index luminal diameter of 3.0±1.3 mm with a minimum diameter of 1.3 mm and a maximum diameter of 6.7 mm. The mean index outer diameter was 5.4±2.1 mm with a minimum diameter of 2.8 mm and a maximum diameter of 11.6 mm. The mean index wall thickness was 1.2±0.5 mm with a minimum thickness of 0.56 mm and a maximum thickness of 2.40 mm. For the manual method, the selected 75 manual match bronchi had a mean luminal

diameter of 2.9±1.1 mm with a minimum diameter of 1.5 mm and a maximum diameter of 5.9 mm. The mean manual match outer diameter was 5.3±2.0 mm with a minimum diameter of 2.8 mm and maximum diameter of 10.7 mm. The mean manual match wall thickness for the selected 75 bronchi was 1.2± 0.5 mm with a minimum wall thickness of 0.6 mm and a maximum wall thickness of 2.4 mm. For the automated method, the 75 selected automatic match bronchi had a mean luminal diameter of 2.9±1.1 mm with a minimum diameter of 1.4 mm and a maximum diameter of 5.9 mm. The mean automated match outer diameter was 5.3±2.0 mm with a minimum diameter of 2.7 mm and maximum diameter of 10.7 mm. The mean automated match wall thickness for the selected 75 bronchi was 1.2±0.5 mm with a minimum wall thickness of 0.6 and a maximum wall thickness of 2.5.

Between reader reliability determined by the Shrout–Fleiss intraclass correlation for the three readers for internal diameter, outer diameter, and wall thickness were 0.993, 0.991, and 0.966 respectively. The mean absolute percentage difference between the manual match airway measurements and the index LDHRCT airway measurements was 9.4±8.5% for the internal diameter, 6.0±4.1% for the outer diameter, and 10.1±9.3% for the wall thickness. The mean absolute percentage difference between the automatic match airway measurements and the index LDHRCT airway measurements was 9.2±8.6% for the inner diameter, 5.8±4.5% for the outer diameter, and 9.9±9.5% for the wall thickness. Two examples of manual and automatic match airways from the 3D spiral volumetric dataset compared to the index LDHRCT airways are presented in Figure 4. The difference in measurements between manual and automated methods was 2.1±1.2% (2.6±1.5% for ID, 1.9±1.0% for OD and 2.0±1.1% for WT), which was significantly less than the interrater variability of 5.1±4.6% (3.5±3.6% for ID, 4.2±2.7% for OD and 7.5±6.0% for WT; $p<0.05$). For ID, OD, and WT measurements, the Schuirmann's two one-sided equivalence test with paired design revealed p values less than 0.025, allowing us to reject the null hypotheses and conclude that there is no significant difference between the two methods. These results provide evidence to conclude that there was no statistically significant difference between manual and automated methods. These results are summarized in Table 1.

The mean time required to match each airway manually for the three raters was 4.2±1.2 min, translating to a mean time per patient of 105 min. In contrast, the mean time for running the automated algorithm was 12±3 seconds each bronchus, translating to a mean time of only 5 min per patient. The difference was statistically significant ($p<0.01$) and represents a substantial time savings for post-processing cases.

DISCUSSION

We have previously developed software for fully automated analysis of the bronchial tree in volumetric spiral (LDSCT) scans of the chest.[42] While the previous algorithm allowed statistical analysis of a large number of measured bronchial segments in serial LDSCT scans, it was unable to accurately match specific bronchi on LDHRCT scans to bronchi in LDSCT scans. We therefore have implemented a novel algorithm enabling accurate matching of bronchi in LDHRCT scans with the same bronchi imaged using LDSCT scans that are 4–16 months apart.

In our validation, the automated matching algorithm achieved results comparable to manual methods with significant decrease in the total processing time. In addition, since the user is not required to perform detailed matching, subjective operator fatigue is likely to be reduced. When compared to interuser variability for manual matching, our method has significantly less variability. This approach will allow monitoring of disease progression by sampling bronchi accurately matched between LDHRCT and LDSCT scans with decreases in overall radiation exposure by as much as 44% (1. 8–2.5 mSv for a LDSCT scan followed by a LDHRCT scan, compared to 3.2–4.4 mSv for two LDSCT scans). This dose reduction will be even greater in patients who receive multiple follow-up scans.

Limitations

In this study, both manual and automated matching techniques generated ID, OD, and WT airway measurements that became minimally reduced with time, compared to the previous scan. The two scans in each patient were separated by 4–16 months. Because airway wall thickness is an

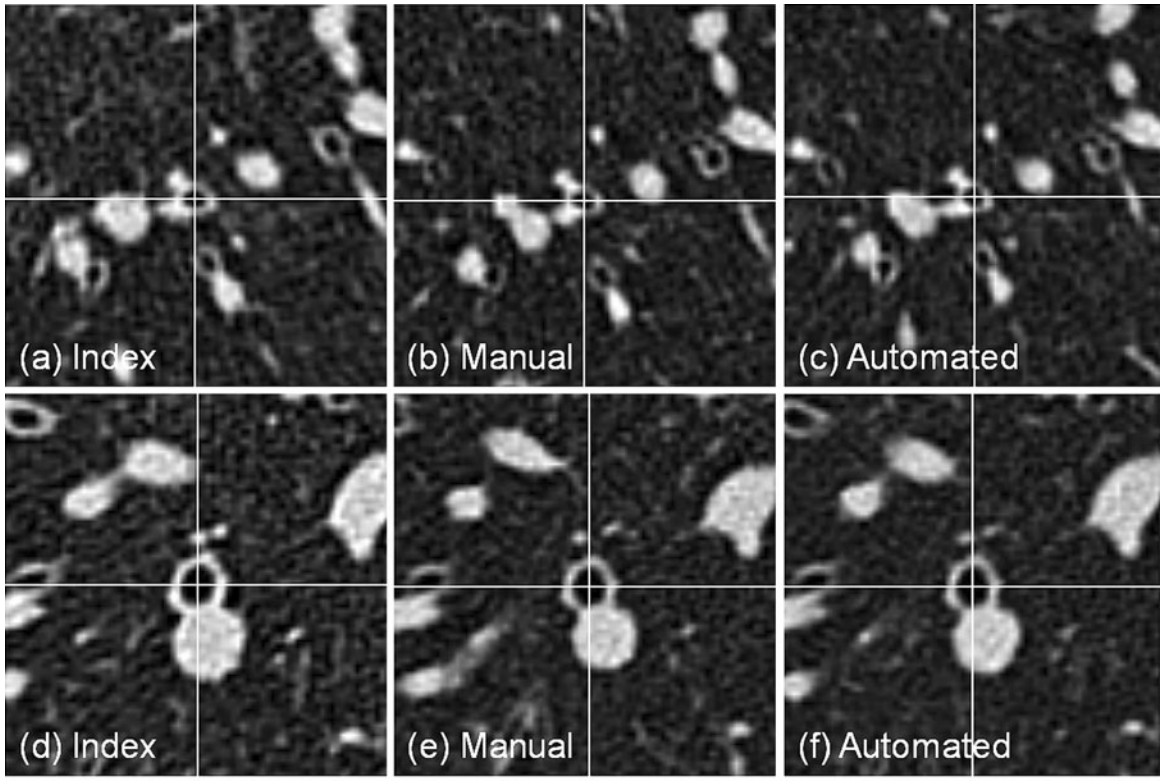

	Airway 1 (a-c)			Airway 2 (d-f)		
	ID	OD	WT	ID	OD	WT
Index	1.92	4.1	1.02	3.63	5.98	1.17
Manual	1.97	4.15	1.09	3.75	6.15	1.2
Automatic	1.98	4.1	1.06	3.83	6.25	1.21

Fig 4. Example matches by manual and automated methods. *ID* internal diameter, *OD* outer diameter, *WT* wall thickness. Index measurement is obtained from LDHRCT scan, and manual and automatic measurements are obtained from the LDSCT scan. Note similar measurement results for manual and automated techniques with less than 3% variability between manual and automated methods.

indirect measure of airway inflammation and airway remodeling, one could expect larger changes in this period of time given the patients' history of CF. In the first two patients, the volumetric scan (obtained on follow-up) showed minimally increased WT, while in the third patient, the HRCT scan (obtained on follow-up) showed minimal increase in WT. The minimal measured

Table 1. Summary of Results

	ID	OD	WT
Mean measurements (mm), index bronchus	3.0 ± 1.3	5.4 ± 2.1	1.2 ± 0.5
Mean measurements (mm), best match bronchus	2.9 ± 1.1	5.3 ± 2.0	1.2 ± 0.5
Mean measurements (mm), automatic match bronchus	2.9 ± 1.1	5.3 ± 2.0	1.2 ± 0.5
Intraclass correlation (manual readers)	0.993	0.991	0.966
Mean absolute percentage difference (manual vs index)	9.4 ± 8.5	6.0 ± 4.1	10.1 ± 9.3
Mean absolute percentage difference (automatic vs index)	9.2 ± 8.6	5.8 ± 4.5	9.9 ± 9.5
Mean absolute percentage interrater variability	3.5 ± 3.6	4.2 ± 2.7	7.5 ± 6.0
Mean absolute percentage difference (automatic vs manual)	2.6 ± 1.5	1.9 ± 1.0	2.0 ± 1.1

changes could be accounted for by two factors. In all three CF subjects, aggressive airway clearance and anti-inflammatory airway therapy have been a regular consistent aspect of their care over several years, which might account for the minimal changes in airway wall thickness. Differences in the lung volume scan acquisition between test dates may also have accounted for the measured differences noted since one subject's HRCT scan was not carefully controlled by spirometer acquisition, and one subject's volumetric scan was obtained at a lower lung volume than the HRCT scan.

The current implementation of our algorithm also requires the user to run the matching algorithm for every index bronchus that needs to be matched, which increases dedicated time for overall evaluation. In the future, it may save time to allow the user to select all bronchi to be matched and then batch review the matched bronchi. This would allow the user to complete other tasks, while the algorithm is running to match all bronchi that are identified.

CONCLUSION

We have developed an algorithm that allows matching of bronchial airways from low-dose HRCT scans with low-dose spiral volumetric chest CT scans to evaluate changes in bronchial morphology in patients with progressive lung disease. This algorithm allows accurate matching of measured airways between scans, allowing small changes in bronchial morphology to be detected. Utilizing this strategy, further reduction in cumulative radiation dose can be achieved while following the progression of chronic lung diseases such as CF in children.

ACKNOWLEDGMENT

Grant support was provided by the Lucille Packard Children's Hospital at Stanford for this project.

REFERENCES

1. Shah RM, Sexauer W, Ostrum BJ, et al: High-resolution CT in the acute exacerbation of cystic fibrosis: evaluation of acute findings, reversibility of those findings, and clinical correlation. AJR Am J Roentgenol 169:375–380, 1997

2. Helbich TH, Heniz-Peer G, Fleischmann D, et al: Evolution of CT findings in patients with cystic fibrosis. AJR Am J Roentgenol 173:81–88, 1999

3. Brody AS, Molina PL, Klein JS, et al: High-resolution computed tomography of the chest in children with cystic fibrosis: support for use as an outcome surrogate. Pediatr Radiol 29:731–735, 1999

4. Robinson TE, Leung AN, Northway WH, et al: Spirometer-triggered high-resolution computed tomography and pulmonary function measurements during an acute exacerbation in patients with cystic fibrosis. J Pediatr 138:553–559, 2001

5. Nasr SZ, Kuhns LR, Brown RW, et al: Use of computerized tomography and chest x-rays in evaluating efficacy of aerosolized recombinant human DNase in cystic fibrosis patients younger than age 5 years: a preliminary study. Pediatr Pulmonol 31:377–382, 2001

6. Robinson TE, Leung AN, Northway WH, et al: Composite spirometric-computed tomography outcome measure in early cystic fibrosis lung disease. Am J Respir Crit Care Med 168:588–593, 2003

7. Robinson TE: High-resolution CT scanning: potential outcome measure. Curr Opinion Pulm Med 10(6):537–541, 2004

8. Moss RB, Rodman D, Spencer LT, et al: Repeated adeno-associated virus serotype 2 aerosol-mediated cystic fibrosis transmembrane regulator gene transfer to the lungs of patients with cystic fibrosis: a multicenter, double-blind, placebo-controlled trial. Chest 125:509–521, 2004

9. de Jong PA, Nakano Y, Lequin MH, et al: Progressive damage on high resolution computed tomography despite stable lung function in cystic fibrosis. Eur Respir J 23(1):93–97, 2004

10. Brody AS, Sucharew H, Campbell JD, et al: Computed tomography correlates with pulmonary exacerbations in children with cystic fibrosis. Am J Respir Crit Care Med 172:1128–1132, 2005

11. de Jong PA, Nakano Y, Hop WC, et al: Changes in airway dimensions on computed tomography scans of children with cystic fibrosis. Am J Respir Crit Care Med 172:218–224, 2005

12. Brody AS, Tiddens HA, Castile RG, et al: Computed tomography in the evaluation of cystic fibrosis lung disease. Am J Respir Crit Care Med 172:1246–1252, 2005

13. de Jong PA, Lindblad A, Rubin , et al: Progression of lung disease on computed tomography and pulmonary function tests in children and adults with cystic fibrosis. Thorax 61:80–85, 2006

14. Tiddens HA, de Jong PA: Update on the application of chest computed tomography scanning to cystic fibrosis. Curr Opinion Pulm Med 12:433–439, 2006

15. Nasr SZ, Gordon D, Sakmar E, et al: High resolution computerized tomography of the chest and pulmonary function testing in evaluating the effect of tobramycin solution for inhalation in cystic fibrosis patients. Pediat Pulmonol 41:1129–1137, 2006

16. Judge EP, Dodd JD, Masterson JB, et al: Pulmonary abnormalities on high-resolution CT demonstrate more rapid decline than FEV1 in adults with cystic fibrosis. Chest 130:1424–1432, 2006

17. Robinson TE: Imaging of the chest in cystic fibrosis. Clin Chest Med 28(2):405–421, 2007 Jun

18. Robinson TE: Computed tomography scanning techniques for the evaluation of cystic fibrosis lung disease. Proc Am Thorac Soc 4(4):310–315, 2007 Aug 1

19. de Jong PA, Tiddens HA: Cystic fibrosis specific computed tomography scoring. Proc Am Thorac Soc 4 (4):338–342, 2007 Aug 1

20. ImPACT Group: CT dosimetry tool. Impact, St. George's Healthcare NHS Trust, London. http://www.impactscan.org/ctdosimetry.htm. Accessed 12 Dec 2008, 2007

21. Huda W, Ogden KM: Computing effective doses to pediatric patients undergoing body CT examinations. Pediatr Radiol 38:415–423, 2008

22. Grenier PA, Beigelman-Aubry C, Fetita C, et al: Multi-detector-row CT of the airways. Semin Roentgenol 38:146–157, 2003

23. Bagheri MH, Hosseini SK, Mostafavi SH, et al: High-resolution CT in chronic pulmonary changes after mustard gas exposure. Acta Radiol 44:241–245, 2003

24. Ooi GC, Khong PL, Chan-Yeung M, et al: High-resolution CT quantification of bronchiectasis: clinical and functional correlation. Radiology 225:663–672, 2002

25. Tiddens HA, de Jong PA: Imaging and clinical trials in cystic fibrosis. Proc Am Thorac Soc 4(4):343–346, 2007 Aug 1

26. Brody AS: Computed tomography scanning in cystic fibrosis research trials: practical lessons from three clinical trials in the United States. Proc Am Thorac Soc 4(4):350–354, 2007 Aug 1

27. Bhalla M, Turcios N, Aponte V, et al: Cystic fibrosis: scoring system with thin-section CT. Radiology 179:783–788, 1991

28. Nathanson I, Conboy K, Murphy S, et al: Ultrafast computerized tomography of the chest in cystic fibrosis: a new scoring system. Pediatr Pulmonol 11:81–86, 1991

29. Maffessanti M, Candusso M, Brizzi F, et al: Cystic fibrosis in children: HRCT findings and distribution of disease. J Thorac Imaging 11:27–38, 1996

30. de Jong PA, Ottink MD, Robben SG, et al: Pulmonary disease assessment in cystic fibrosis: comparison of CT scoring systems and value of bronchial and arterial dimension measurements. Radiology 231:434–439, 2004

31. Moskowitz SM, Gibson RL, Effmann EL: Cystic fibrosis lung disease: genetic influences, microbial interactions, and radiological assessment. Pediatr Radiol 35:739–757, 2005

32. Brody AS, Kosorok MR, Li Z, et al: Reproducibility of a scoring system for computed tomography scanning in cystic fibrosis. J Thorac Imaging 21:14–21, 2006

33. Long FR, Williams RS, Castile RG: Structural airway abnormalities in infants and young children with cystic fibrosis. J Pediatr 144:154–161, 2004

34. Martinez TM, Llapur CJ, Williams TH, et al: High-resolution tomography imaging of airway disease in infants with cystic fibrosis. Am J Respir Crit Care Med 172:1133–1138, 2005

35. Goris ML, Zhu HJ, Blankenberg F, et al: An automated approach to quantitative 2 air trapping measurements in mild cystic fibrosis. Chest 123:1655–1663, 2003

36. Bonnel AS, Song SM, Kesavaraju K, et al: Quantitative air trapping analysis in children with mild cystic fibrosis pulmonary disease. Pediatr Pulmonol 38:396–405, 2004

37. Robinson TE, Goris ML, Zhu HJ, et al: Changes in quantitative air trapping, pulmonary function, and chest HRCT scores in CF children during a Pulmozyme intervention study. Chest 128:2327–2335, 2005

38. Nakano Y, Muro S, Sakai H, et al: Computed tomographic measurements of airway dimensions and emphysema in smokers. Correlation with lung function. Am J Respir Crit Care Med 162:1102–1108, 2000

39. King GG, Muller NL, Whittall KP, et al: An analysis algorithm for measuring airway lumen and wall areas from high-resolution computed tomography data. Am J Respir Crit Care Med 161:574–580, 2000

40. Nakano Y, Whittall KP, Kalloger SE, et al: Development and validation of human airway analysis algorithm using multidetector row CT. SPIE 4683:460–469, 2002

41. Tschirren J, Palagyi K, Hoffman EA, et al: Segmentation, skeletonization, and brnchpoint matching; a fully automated quantitative evaluation of human intrathoracic airway trees. In: Dohi T, Kikinis R Eds. Proceedings of the Fifth International Conference on Medical Image Computing and Computer Assisted Intevention, 2002, Tokyo, Japan. Berlin: Springer, 2002, pp. 12–19

42. Tschirren J, Hoffman EA, McLennan, et al: Branchpoint labeling and matching in humn airway trees. In: Clough AVA, Amir A Eds. Proceedings of the SPIE Medical Imaging 2003, San Diego, CA, 2003, pp 187–194

43. Nakano Y, Wong JC, de Jong PA, et al: The prediction of small airway dimensions using computed tomography. Am J Respir Crit Care Med 171(2):142–146, 2005

44. Tschirren J, Hoffman EA, McLennan , et al: Intrathoracic airway trees: segmentation and airway morphology analysis from low dose CT scans. IEEE Trans Med Imaging 24:1529–1539, 2005

45. Venkatraman R, Raman R, Raman B, et al: Fully automated system for three-dimensional bronchial morphology analysis using volumetric multidetector computed tomography of the chest. Journal of Digial Imaging 19(2):132–139, 2006

46. Dame Carroll JR, Chandra A, Jones AS, et al: Airway dimensions measured from micro-computed tomography and high-resolution computed tomography. Eur Respir J 28(4):712–720, 2006

47. Little SA, Sproule MW, Cowan MD, et al: High resolution computed tomographic assessment of airway wall thickness in chronic asthma: reproducibility and relationship with lung function and severity. Thorax 57:247–253, 2002

48. Gono H, Fujimoto K, Kawakami S, et al: Evaluation of airway wall thickness and air trapping by HRCT in asymptomatic asthma. Eur Respir J 22:965–971, 2003

49. Suter M, Tschirren J, Reinhardt J, et al: Evaluation of the human airway with multi-detector x-ray-computed tomography and optical imaging. Physiol Meas 25:837–847, 2004

50. Takao H, Doi I, Tateno M: Evaluation of an automated system for temporal subtraction of thin-section thoracic CT. Br J Radiol 80:85–89, 2006

51. Sundaram TA, Gee JC: Towards a model of lung biomechanics: pulmonary kinematics via registration of serial lung images. Med Image Anal 9:524–537, 2005

52. Schreibmann E, Xing L: Image registration with auto-mapped control volumes. Med Phys 33:1165–1179, 2006

53. Reeves AP, Chan AB, Yankelevitz DF, et al: On measuring the change in size of pulmonary nodules. IEEE Trans Med Imaging 25:435–450, 2006

54. Danilouchkine MG, Westenberg JJ, van Assen HC, et al: 3D model-based approach to lung registration and prediction of respiratory cardiac motion. Med Image Comput Comput Assist Interv Int Conf Med Image Comput Comput Assist Interv 8:951–959, 2005

55. Coselmon MM, Balter JM, McShan DL, et al: Mutual information based CT registration of the lung at exhale and inhale breathing states using thin-plate splines. Med Phys 31:2942–2948, 2004

56. Betke M, Hong H, Thomas D, et al: Landmark detection in the chest and registration of lung surfaces with an application to nodule registration. Med Image Anal 7:265–281, 2003

57. Shrout PE, Fleiss JL: Intraclass correlations; uses in assessing rater reliability. Psychological Bulletin 86(2):420–428, 1979

58. Schuirmann DJ: A comparison of the two one-sided tests procedure and the power approach for assessing the equivalence of average bioavailability. J Pharmacokinet Biopharm 15 (6):657–680, 1987